Table 1 Numerical values

α	$= 4 \cdot 10^{-4}(°K)^{-1}$
β	$= 14 \cdot 10^{-4}(°K)^{-1}$
u_1	$= 2 \cdot 07 \cdot 10^{-2}$ cm/sec·atm$^{2/3}$
ν	$= 2/3$
T_0	$= 300°K$
k	$= 0 \cdot 8 \cdot 10^{-3}$ cm^2/sec
T_s	$= 600°K$

in a powder specimen with a moving boundary (combustion front).

As the first approximation, we suppose that the temperature profile under the extinction is a linear one

$$\zeta^* = (T_s - T_c)/h \tag{7}$$

where T_c is temperature at the powder-metal contact and h is the powder layer thickness at the moment of extinction.

The thermal conductivity and the mass of the metal plate are very great. Therefore, we can assume that the temperature of a powder-metal contact is constant.

One can calculate the value of the unburned powder slab thickness, h, from Eqs. (5) and (7) if one knows the values of k, T_s, T_c, T_0^*, and u^*. The corresponding formula is

$$h = k(T_s - T_c)/u^*(T_s - T_0^*) \tag{8}$$

The temperature of a powder-metal contact T_c equals room temperature. The values of powder thermal diffusivity and of the temperature of a burning powder surface can be taken from Refs. 8 and 9.

Utilizing the solution of Eq. (6) in Eqs. (3) and (8) and substituting corresponding numerical values from Table 1, one finds the relationship between the thickness of unburned powder and pressure. This relationship has the form

$$\ln h = -3.95 - \nu \ln p \tag{9}$$

The theoretical line (9) is represented by a dotted line in Fig. 1. As the figure shows, the agreement between the theoretical result and the experimental one is good.

For a more rigorous comparison of theory and experiment, the following facts must be kept in mind. 1) The metal thermal conductivity is high but finite, and during the burning the temperature of metal-powder interface does not remain constant. 2) The burning surface temperature depends on pressure. 3) The empirical relation between the steady burning rate and pressure and initial temperature in the form (3) is approximate, and the extinction criterion (5) is not quite accurate.

The method presented can be used also to obtain reliable experimental data on the dependence of the unburned layer powder thickness on initial temperature.

It should be noted that there is at present no correct nonsteady combustion theory that deals with combustion instability, ignition, and extinction.[10] The method presented can be useful in investigation of the extinction and for verification of nonsteady combustion theories.

References

[1] Ciepluch, C. C., "Effect of Rapid Pressure Decay on Solid Propellant Combustion," *ARS Journal*, Vol. 31, No. 11, Nov. 1961, p. 1584.

[2] Slocum, R. W., "Results of Solid Rocket Motor Extinguishing Experiments," *AIAA Journal*, Vol. 1, No. 6, June 1963, pp. 1419–1420.

[3] Andreev, K. K., *The Thermic Decomposition and Combustion of Explosives*, Izdatel'stvo "Nauka," Moscow, 1966, pp. 109–123.

[4] Zeldovich, J. B., "On the Combustion Theory of Powder and of the Explosives," *Zhurnal Eksperimental'noi i Teoreticheskoi Fiziki*, Vol. 12, No. 11–12, 1942, p. 498.

[5] Zeldovich, J. B., "On a Burning Rate under Nonsteady Pressure," *Zhurnal Prikladnoi Mekhaniki i Technicheskoi Fiziki*, No. 3, Jan.-Feb. 1964, pp. 126–130.

[6] Pokhil, P. F., Nefedova, O. I., and Morgolin, A. D., "Anomalous Dependence of Powder Burning Rate on Initial Temperature," *Doklady Akademii Nauk SSSR*, Vol. 142, No. 4, 1962, pp. 860–862.

[7] Korotkov, A. I. and Leypunski, O. I., "The Dependence of a Temperature Coefficient of the Powder Burning Rate on Temperature under Normal Pressure," *Zbornik "Fizika vzriva,"* Izdatel'stvo "Nauka," No. 2, 1953, pp. 31–35.

[8] Gostintsev, Y. A. and Morgolin, A. D., "On the Nonsteady Propellant Combustion under Influence of a Pressure Impulse," *Zhurnal Firika Goreniya i Vzriva*, Vol. 1, No. 2, 1965, pp. 69–74.

[9] Alkesandrov, V. V. et al., "On the Burning Surface Temperature of the Nitroglycerine Powder," *Zhurnal Firika Goreniya i Vzriva*, Vol. 2, No. 1, 1966, pp. 68–73.

[10] Summerfield, M. and Krier, H., "Errors in Nonsteady Combustion Theory in the Past Decade," AIAA Paper 69-178, New York, 1969.

Effect of Eccentricity on the Attitude Stability of a Nonspinning Satellite

H. D. NELSON*
Arizona State University, Tempe, Ariz.
AND
L. E. WESSON†
Sperry Flight Systems Division, Phoenix, Ariz.

RECENTLY, considerable attention has been given to the study of the attitude of a rigid body carrying a rotor that can rotate relative to an axis fixed in the body. Of the several papers that have been published pertaining to this subject, two are of particular interest in this Note. Kane and Barba[1] studied the influence of orbit eccentricity on the attitude stability of a spinning, symmetric satellite. Their study revealed that an increase in eccentricity tended to cause existing instability regions of a nondimensional system parameter space to grow; also, new regions of instability occurred in regions where instabilities were not encountered for circular orbits. Shippy and Robe[2] studied the influence of a spherical rotor on the attitude stability of a nonspinning, symmetric satellite in a circular orbit. The spin axis of the rotor was placed perpendicular to the symmetry axis of the satellite and the symmetry axis was perpendicular to the orbit plane for the reference motion. Their study revealed that the inclusion of a laterally oriented rotor, spinning at a constant rate s, acts either as a stabilizer or destabilizer depending on the point in the system parameter space.

The purpose of this Note is to present a generalized study of the work by Shippy and Robe by including the effect of orbit eccentricity, ϵ. By utilizing the usual assumption of independence of mass center motion to attitude motion, the nondimensionalized orbit equations for the satellite-rotor mass center are[1]

$$\zeta'' + \zeta^{-3}(\epsilon^2 - 1) + \zeta^{-2} = 0$$
$$\theta' = (1 - \epsilon^2)^{1/2}\zeta^{-2} \tag{1}$$

The prime denotes differentiation with respect to the scaled time, $\tau = nt$, and $\zeta = r/a$ is a nondimensional radial position. The "mean motion," n, is defined in terms of the period T as $n = 2\pi/T$; a is the semimajor axis of the orbit; and θ is the orbit angle from the perigee. By utilizing the attitude angles $(\theta_1, \theta_2, \theta_3)$ relative to a rotating orbit triad,[2] the absolute

Received April 1, 1969; revision received September 29, 1969.

* Associate Professor of Engineering Sciences. Member AIAA.

† Project Engineer. Member AIAA.

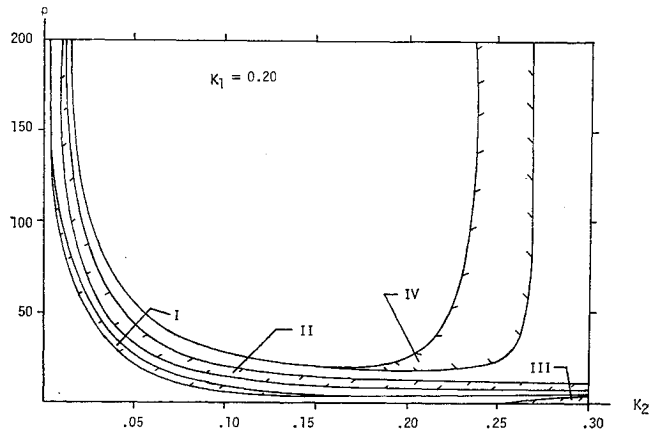

Fig. 1 ϵ = 0.01 parameter plane.

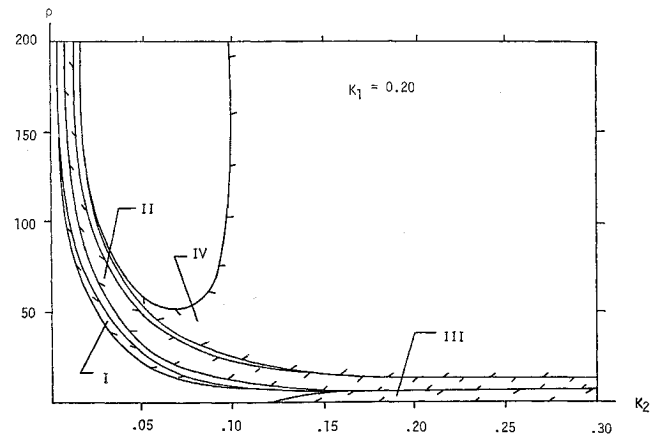

Fig. 3 ϵ = 0.10 parameter plane.

angular velocity components and gravity moment components referred to a principle body triad are

$$\omega_1/n = u_1 = (\theta'_1 C\theta_2 - \theta' C\theta_1 S\theta_2)C\theta_3 + (\theta'_2 + \theta' S\theta_1)S\theta_3$$

$$\omega_2/n = u_2 = -(\theta'_1 C\theta_2 - \theta' C\theta_1 S\theta_2)S\theta_3 + (\theta'_2 + \theta' S\theta_1)C\theta_3 \quad (2)$$

$$\omega_3/n = u_3 = \theta'_1 S\theta_2 + \theta' C\theta_1 C\theta_2 + \theta'_3$$

and

$$M_1/n^2 = 3\zeta^{-3}(I_1 - I_3)S\theta_2 C\theta_2 S\theta_3$$

$$M_2/n^2 = 3\zeta^{-3}(I_1 - I_3)S\theta_2 C\theta_2 C\theta_3 \quad (3)$$

$$M_3/n^2 = 0$$

where I_1 and I_3 are the principal moments of inertia of the satellite.

The nondimensionalized Euler equations governing the attitude motion of the satellite are

$$u'_1 + \frac{K_1}{1+K_2} u_2 u_3 - \frac{K_2\rho}{1+K_2} u_3 = -\frac{3K_1}{1+K_2} \zeta^{-3} S\theta_2 C\theta_2 S\theta_3$$

$$u'_2 - \frac{K_1}{1+K_2} u_1 u_3 = -\frac{3K_1}{1+K_2} \zeta^{-3} S\theta_2 C\theta_2 C\theta_3 \quad (4)$$

$$u'_3 + [K_2\rho/(1 + K_1 + K_2)]u_1 = 0$$

where the following nondimensional system parameters have been introduced using J as the moment of inertia of the spherical rotor:

$$K_1 = (I_3 - I_1)/I_1,\ K_2 = J/I_1,\ \rho = s/n$$

It can be seen that a reference motion for the set of equations (2, 4) is $u_1 = u_2 = u_3 = \theta_1 = \theta_2 = 0$, $\theta_3 = -\theta$. If the variations of the nondimensional angular velocity components (u_1,u_2,u_3) and attitude angles $(\theta_1,\theta_2,\theta_3)$ are defined as (y_1,y_2,y_3) and (y_4,y_5,y_6) respectively, the variational equations associated with the reference motion are

$$\begin{Bmatrix} y'_1 \\ y'_2 \\ y'_3 \\ y'_4 \\ y'_5 \\ y'_6 \end{Bmatrix} = \begin{Bmatrix} 0 & 0 & \frac{K_2\rho}{1+K_2} & 0 & \frac{3K_1 S\theta}{\zeta^3(1+K_2)} & 0 \\ 0 & 0 & 0 & 0 & \frac{-3K_1 C\theta}{\zeta^3(1+K_2)} & 0 \\ \frac{-K_2\rho}{1+K_1+K_2} & 0 & 0 & 0 & 0 & 0 \\ C\theta & S\theta & 0 & 0 & \theta' & 0 \\ -S\theta & C\theta & 0 & -\theta' & 0 & 0 \\ 0 & 0 & 1 & 0 & 0 & 0 \end{Bmatrix} \begin{Bmatrix} y_1 \\ y_2 \\ y_3 \\ y_4 \\ y_5 \\ y_6 \end{Bmatrix} \quad (5)$$

In accordance with the analysis by Shippy and Robe, the first

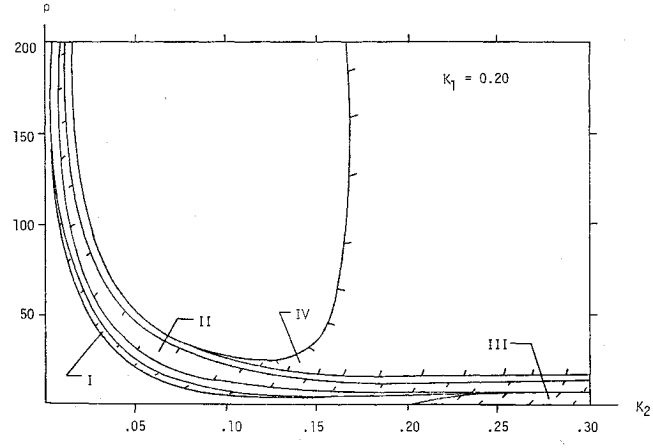

Fig. 2 ϵ = 0.05 parameter plane.

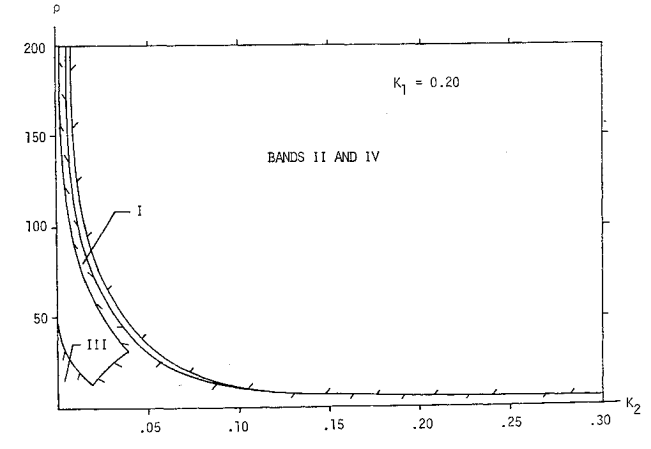

Fig. 4 ϵ = 0.20 parameter plane.

five variational equations of (5) form a complete set of linear equations with periodic coefficients to which Floquet theory[3] may be applied to study stability in the small of the attitude motion of the satellite symmetry axis.

The system parameter space is of dimension four with components K_1, K_2, ρ, and ϵ. In this study the parameter K_1 was held at the constant value 0.20 and the remaining parameters were varied over the ranges $0 < K_2 < 0.30$, $0 < \rho < 200$, and $0 < \epsilon < 0.25$. The results of the Floquet analysis for four planes associated with constant values of $\epsilon = 0.01, 0.05, 0.10$, and 0.20 are shown in Figs. 1, 2, 3, and 4 respectively. The influence of orbit eccentricity in this study is qualitatively similar to the results obtained by Kane and Barba. For a circular orbit, $\epsilon = 0$, there are two unstable bands in the (ρ,K_2) plane, as was determined by Shippy and Robe. As ϵ is increased, these bands labeled I and II, gradually widen and two additional unstable regions, labeled III and IV, appear where the motion was previously stable for a circular orbit. Figures 1, 2, 3, and 4 illustrate that the unstable regions (I and III) and (II and IV) tend to merge with increasing ϵ. Finally, at $\epsilon \simeq 0.25$, the entire (ρ,K_2) plane, with the exception of a very narrow band separating the (I,III) and (II,IV) regions, corresponds to unstable attitude motion.

References

[1] Kane, T. R. and Barba, P. M., "Attitude Stability of a Spinning Satellite in an Elliptic Orbit," *Journal of Applied Mechanics*, Vol. 33, No. 2, June 1966, pp. 402–405.

[2] Shippy, D. J. and Robe, T. R., "Effect of a Rotor on the Attitude Stability of a Non-Spinning Symmetrical Satellite," Fourth Southeastern Conference on Theoretical and Applied Mechanics, New Orleans, La., Feb. 29–March 1, 1968.

[3] Coddington, E. L. and Levinson, N., *Theory of Ordinary Differential Equations*, McGraw-Hill, New York, 1955, pp. 78–81.

Collapse Loads of Partially Loaded Clamped Shallow Spherical Caps

C. E. Dumesnil*
Vought Aeronautics Division, LTV Aerospace Corporation, Dallas, Texas

AND

G. E. Nevill Jr.†
University of Florida, Gainesville, Fla.

In 1968, Lee and Onat[1] gave an exact solution for collapse loads of uniformly loaded axially symmetric spherical shells of a rigid-plastic material which obeys the Tresca yield condition and flow law. This Note extends their work to caps with a uniform axially symmetric partial load. The nomenclature is that of Ref. 1 except that φ replaces S.

Stress Field

The equations of equilibrium for the cap, from Ref. 1 are

$$\begin{aligned} n'_\varphi &= [n_\theta - n_\varphi - (n_\varphi + p)\tan^2\varphi]\cot\varphi \\ m'_\varphi &= [m_\theta - m_\varphi - (1/k)(n_\varphi + p)\tan^2\varphi]\cot\varphi \end{aligned} \tag{1}$$

Received June 16, 1969; revision received October 2, 1969. The authors express their appreciation to NASA for support of this research under Grant NGR 10-005-036.

* Engineering Specialist.

† Professor, Department of Engineering Science and Mechanics, College of Engineering.

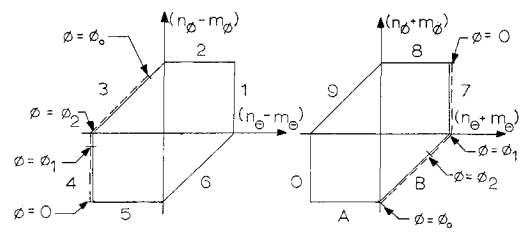

Fig. 1 Yield surface for clamped cap.

for the loaded region of the cap, $0 \le \varphi \le \varphi_L$, and

$$\begin{aligned} n'_\varphi &= \left[n_\theta - n_\varphi - n_\varphi\tan^2\varphi - p\,\frac{\sin^2\varphi_L}{\cos^2\varphi}\right]\cot\varphi \\ m'_\varphi &= \left[m_\theta - m_\varphi - \frac{1}{k}\,n_\varphi\tan^2\varphi - \frac{1}{k}\,p\,\frac{\sin^2\varphi_L}{\cos^2\varphi}\right]\cot\varphi \end{aligned} \tag{2}$$

for the unloaded region of the cap, $\varphi_L \le \varphi \le \varphi_0$.

The Tresca sandwich yield surface is represented in Fig. 1. The analysis begins by choosing a collapse pressure p^* and determining an appropriate stress state at the center of the shell. Following Ref. 1, the starting point on the yield surface is chosen as the intersection of faces 45 and 78. The stress point then moves along face 47 on which $n_\theta = 0$ and $m_\theta = 1$. Utilizing these conditions and the initial conditions $n_\varphi = 0, m_\varphi = 0$ at $\varphi = 0$, Eqs. (1) are solved to obtain

$$n_\varphi = -p^*(1 - \varphi\cot\varphi),\ m_\varphi = 1 - (1/k)p^*(1 - \varphi\cot\varphi) \tag{3}$$

for the region $0 \le \varphi \le \varphi_1$. The stress point motion on 47 is interrupted when 7B is reached, where $n_\varphi + m_\varphi = 0$. This condition, with Eqs. (3), is used to determine φ_1.

If plastic deformation is to occur everywhere, further motion of the stress point must be along 4B, where the conditions $m_\theta = 1 + n_\theta$ and $n_\varphi = \frac{1}{2}(n_\varphi + m_\varphi)$ hold. These conditions, combined with Eqs. (1), yield the second-order differential equation

$$n''_\varphi + n'_\varphi\left[\frac{2}{\sin\varphi\cos\varphi}\right] + n_\varphi\left[2\sec^2\varphi + \frac{1}{2}\left(\frac{1+k}{k}\right)\right] = \frac{1}{2}\cot^2\varphi - p^*\left[2\sec^2\varphi + \frac{1}{2}\left(\frac{1+k}{k}\right)\right] \tag{4}$$

This equation was solved numerically using a fourth-order Runge-Kutta stepping method,[2] with initial conditions on n_φ at φ_1 obtained from Eq. (3). The motion on 4B continues to corner 34. This point, φ_2, is determined by the condition $n_\varphi - m_\varphi = 0$. The stress point then moves on 3B, where $n_\theta = n_\varphi$ and $m_\theta = 1 + m_\varphi$. This condition, with Eqs. (1), allows the solution, in the region $\varphi_2 \le \varphi \le \varphi_L$,

$$\begin{aligned} n_\varphi &= C_1\cos\varphi - p^* \\ m_\varphi &= \ln(\sin\varphi) + (1/k)C_1\cos\varphi + C_2 \end{aligned} \tag{5}$$

C_1 and C_2 are determined by requiring continuity at φ_2.

For $\varphi \ge \varphi_L$, the cap is unloaded and further motion on 3B is controlled by Eqs. (2). With the requirements of 3B, (2) yields

$$\begin{aligned} n_\varphi &= C_3\cos\varphi - p^*\sin^2\varphi_L[1 + \cos\varphi\ln(\tan\varphi/2)] \\ m_\varphi &= \ln(\sin\varphi) + (1/k)C_3\cos\varphi - (1/k)p^*\sin^2\varphi_L \times \\ &\qquad \cos\varphi\ln\{\tan(\varphi/2)\} + C_4 \end{aligned} \tag{6}$$

C_3 and C_4 are determined from continuity conditions at $\varphi = \varphi_L$. The stress point continues on 3B to the corner AB where $-n_\varphi - m_\varphi = 1$. The angle $\varphi = \varphi_0$ where this occurs is a possible location for the clamped edge of the cap. Thus, a statically admissible stress field has been obtained and the chosen p^* is a lower bound on the collapse pressure for a shell with half opening angle φ_0.